

Inverse-designed CWDM demultiplexer operated in O-band

Alfred K. C. Cheung¹, Krishna Gadepalli¹, Jian Guan¹, Andreas Hoenselaar¹, Yang Meng¹, Anton Menshov¹, Jan Petykiewicz², Xavier Serey¹, Rhett Stucki¹, Lieven Verslegers², Jiahui Wang¹, Phil Watson¹, Ian A. D. Williamson¹, and Yi-Kuei Ryan Wu^{1,*†}

¹*X the moonshot factory, 100 Mayfield Ave, Mountain View, California, USA, 94043*

²*Google LLC, 1600 Amphitheatre Parkway, Mountain View, CA 94043*

**yikueiryawu@x.team*

†*Authors appear in alphabetical order.*

Abstract: We introduce an inverse designed silicon 4-channel CWDM demux with mean worst insertion loss of 2-3.3 dB and mean worst crosstalk of 19-26 dB. Variability and predictability are demonstrated using a commercial CMOS process.

1. Introduction

Inverse-designed photonics is a new approach to designing photonic devices. Instead of starting with a desired device physics based on designers' intuition and then designing a device to achieve that performance, inverse-designed photonics starts with the desired device performance and then uses optimization algorithms to find a device design that meets that performance. This approach has the potential to lead to new and innovative photonic devices that are not possible with conventional design methods. There have been many exciting developments in academic research [1-3].

However, inverse-designed photonics face challenges of the device performance predictability and the device variability. Because the inverse-designed photonic components often consist of non-intuitive patterns, it adds the complexity of the fabrication to reproduce these non-intuitive patterns. Therefore, inverse-designed photonic components need to be able to demonstrate the device performance predictability and the device variability.

In this paper, we select a CWDM demultiplexer (DEMUX) as a problem to demonstrate the device variability and the device performance predictability.

2. Device Design

In order to demonstrate real world relevance, we start with a CWDM4 demux (4 channel coarse wavelength division multiplexing demultiplexer), where the wavelength targets are 1270nm, 1290nm, 1310nm, and 1330nm (O-band).

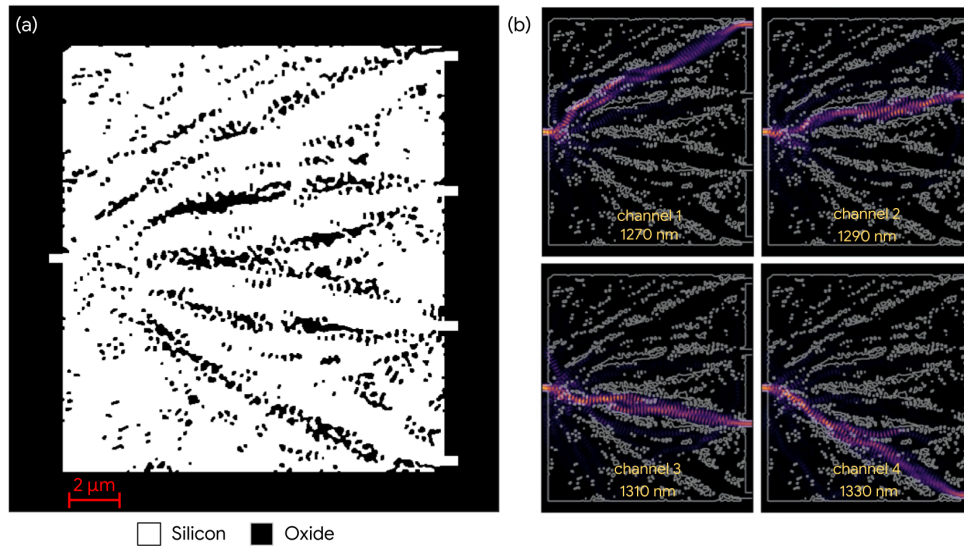


Fig. 1. (a) The 14x16 μm design of the CWDM4 demux obtained using the design methodology in [4]. The white material represents silicon and the black material is silicon oxide. (b) The energy intensity at the center wavelength

of each channel, corresponding to wavelengths of 1270 nm, 1290 nm, 1310 nm, and 1330 nm. The gray contour indicates the material interface between silicon and silicon oxide.

The device is designed on an SOI wafer, where the thickness of the silicon is based on the foundry PDK. The design is optimized using the topology optimization method introduced in [4], with a $14 \times 16 \mu\text{m}$ design region discretized at a design pixel size of 10nm. Strict length scale design constraints are enforced using a non-differentiable conditional generator for constrained designs, and a straight-through estimator [5] for enabling backpropagation through the generator. Electromagnetic simulations of components are performed using a finite difference time domain (FDTD) solver [6]. The resulting design, shown in Fig. 1(a), is compliant everywhere with design rule checks imposed by the commercial CMOS foundry. The energy intensity at wavelengths of 1270 nm, 1290 nm, 1310 nm, and 1330 nm are shown in Fig. 1(b).

3. Experimental results

The devices were fabricated in a passive flow at GlobalFoundries using their 45SPCLO silicon photonics process. Measurements were carried out using a wafer-level tester, where a laser source swept through different wavelengths and a photodiode detected the corresponding output signal. Initially, a grating reference measurement was performed, followed by the measurement of the device under test (DUT). The spectra of the DUT were de-embedded by subtracting the grating reference measurement.

Fig. 2(a) illustrates a comparison between simulation and measurement. Here, the thick solid lines represent the simulated spectra of the four channels of the DEMUX, while the dashed lines represent the measured spectra of these channels. Overall, there is good agreement between the simulation and measurement, indicating high predictability in device performance.

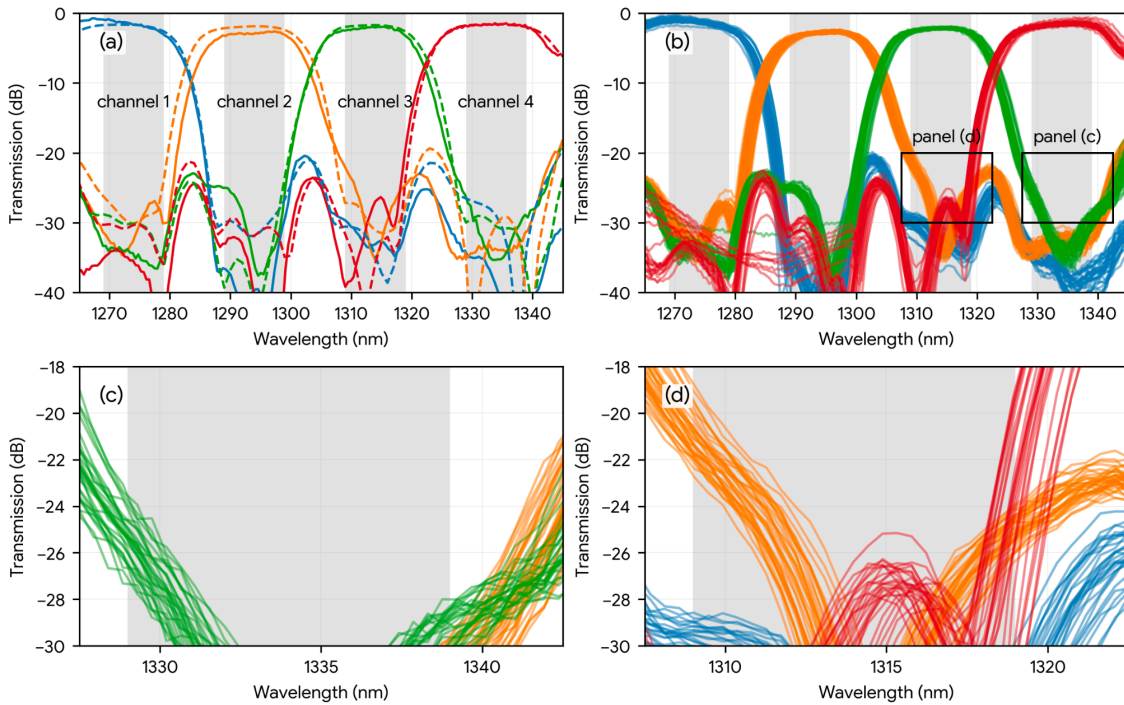


Fig. 2. (a) Measured (solid) and simulated (dashed) transmission spectra for a single chip. (b) Measured transmission spectra from 34 chips. (c-d) Enlarged view of measured transmission spectra across channel 3 and channel 4.

To further illustrate device variability, we overlay spectra from 34 chips in Fig. 2(b). Additionally, Fig. 2(c) and Fig. 2(d) provide zoomed-in views of Fig. 2(b). Fig. 2(c) focuses on the red channel (channel 4), showcasing excellent performance in terms of crosstalk and a strong match between simulation and measurement. Conversely, Fig. 2(d)

focuses on the green channel (channel 3), which exhibits the highest crosstalk among all channels and a notable deviation between simulation and measurement. Irrespective of performance disparities, both Fig. 2(c) and Fig. 2(d) demonstrate remarkably consistent measured results across the 34 chips.

Fig. 3 further extracts the DEMUX metrics from the measured results in Fig. 2(c). The channel wavelength shift in relation to the channel target wavelengths across these 34 chips has mean of 4.2nm, where the one sigma of this distribution is 0.67nm. After the mean wavelength offset is corrected in the next tapeout, the one sigma for the channel wavelength target off spread is expected to remain the same. Regarding the variation of the wavelength shift, it can be compensated with a low power heater. Fig. 3(a) displays the worst insertion loss with respect to the channel number, with the mean ranging 2-3.3dB. It is evident that improvements are needed for channel 2 (yellow channel) and channel 3 (green channel) to achieve better insertion loss. Nevertheless, even in the case of the worst insertion loss, the one sigma distribution is 0.41dB. Fig. 3(b) provides statistics on the worst crosstalk, showing a mean ranging 19-26dB. As observed in Fig. 2(d), the crosstalk in channel 3 (green channel) experiences degradation due to simulation-measurement deviation, highlighting the need for improvement. Nonetheless, the crosstalk distribution remains at 0.62dB for one sigma. In summary, Fig. 3 emphasizes that the variability in the inverse-designed photonic device is reasonably low, promising a viable path for future production.

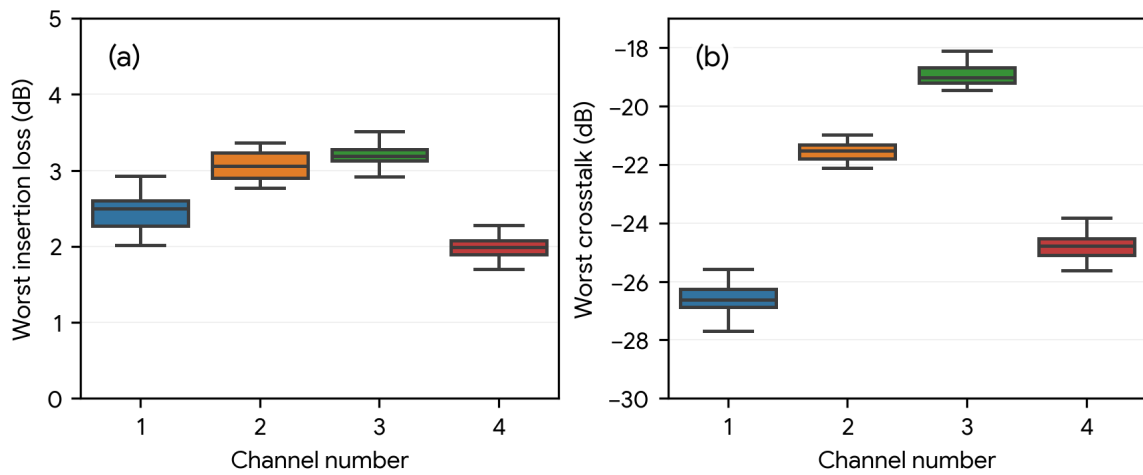


Fig. 3. Measured (a) worst insertion loss and (b) worst crosstalk across 34 chips for each channel.

4. Conclusion

In this paper, we demonstrate our inverse-design methodology, the inverse-designed device performance predictability, and its variability. In summary, it is possible in our design flow to manufacture inverse-designed photonic devices with predictable performance and reasonably low variability. This is a key step towards making inverse-designed photonics a viable technology for mass production.

5. References

- [1] T. Van Vaerenbergh, S. Hooten, M. Jain, P. Sun, Q. Wilmart, A. Seyedi, Z. Huang, M. Fiorentino, and R. Beausoleil, "Wafer-level testing of inverse-designed and adjoint-inspired dual layer Si-SiN vertical grating couplers," *J. Phys. Photonics* **4**(4), 044001 (2022).
- [2] Yang, K.Y., Shirpurkar, C., White, A.D. et al. "Multi-dimensional data transmission using inverse-designed silicon photonics and microcombs," *Nat Commun* **13**, 7862 (2022).
- [3] A. M. Hammond, J. B. Slaby, M. J. Probst, and S. E. Ralph, "Multi-layer inverse design of vertical grating couplers for high-density, commercial foundry interconnects," *Opt. Express* **30**(17), 31058–31072 (2022).
- [4] Martin F. Schubert, Alfred K. C. Cheung, Ian A. D. Williamson, Aleksandra Spyra, and David H. Alexander, "Inverse Design of Photonic Devices with Strict Foundry Fabrication Constraints," *ACS Photonics* **9** (7), 2327-2336 (2022).
- [5] Y. Bengio, N. Léonard, A. Courville, "Estimating or Propagating Gradients Through Stochastic Neurons for Conditional Computation," arXiv:1308.3432 [cs.LG] (2013).
- [6] A. Taflov, S. C. Hagness, "Computational Electrodynamics: The Finite-Difference Time-Domain Method," 3rd ed., Artech, Norwood, MA (2005).